

pubs.acs.org/JPCB Article

Ionic Liquid Aggregation Mechanism for Nanoparticle Synthesis

Kristin Bryant, Ellis Hammond-Pereira, and Steven R. Saunders*



Cite This: J. Phys. Chem. B 2021, 125, 253-263

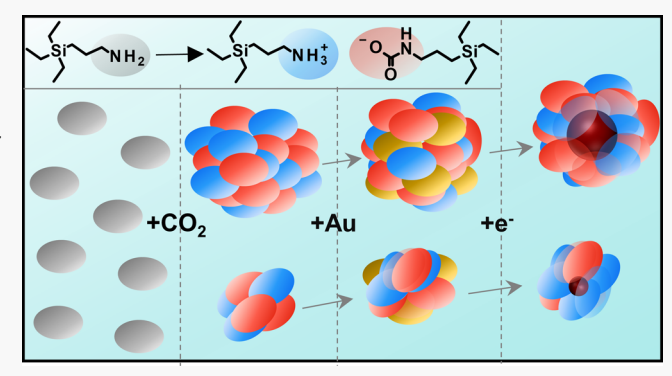


ACCESS I

Metrics & More

Article Recommendations

ABSTRACT: Nanoparticle synthesis with silylamine reversible ionic liquids (RevILs) has been previously demonstrated to offer unique alternatives to traditional nanoparticle syntheses, allowing for size control and facile deposition onto support surfaces via the switchable nature of the IL. However, the mechanism of nanoparticle synthesis remains uncharacterized. The use of RevILs facilitates the synthesis of size-controlled nanoparticles without the use of additional stabilizing agents (i.e., surfactants, ligands, and polymers) that passivate the nanoparticle surface, which are traditionally required to control the nanoparticle size. Traditional techniques often require harsh activation steps that ultimately impact nanoparticle size and morphology. While RevIL syntheses offer an excellent alternative, as they do not require additional



activation steps, the mechanism through which nanoparticles are synthesized in these systems has not been studied previously. Preceding work hypothesized nanoparticles prepared with RevILs are formed via a reverse micelle mechanism, in which nanoparticles are stabilized and templated within the aqueous core of the organized micelle structures. In this work, DOSY-NMR is used to demonstrate that nanoparticles synthesized with 3-aminopropyltriethylsilane RevIL are not formed through a reverse micelle mechanism but rather a switchable aggregation mechanism that affords control over the nanoparticle size via manipulation of the RevIL structure and concentration. Furthermore, it is shown that the addition of water to RevIL systems has detrimental effects on the aggregation behavior of the ionic liquid molecules in solution, causing disassembly of the ion pairs. However, because nanoparticle reduction likely occurs faster than the disassembly of the ion pairs, nanoparticle size is unaffected by the addition of water during nanoparticle reduction.

■ INTRODUCTION

Metallic colloidal nanoparticles are of interest in a variety of modern applications including fuel cells, biomedicine, 2,3 data storage, 4 solar cells, 5 agriculture, 6 and catalysis. 7,8 Developing synthesis methods that allow for fine control over nanoparticle size and morphology is extremely important because of their unique size-dependent properties at the nanoscale. 9-12 It is essential to understand the process of nanoparticle formation in order to design size-controlled syntheses. Some of the most common synthesis methods include chemical "bottom-up" approaches, in which metallic salts are chemically reduced and nanoparticles are formed through classical nucleation and growth. The vast majority of these techniques require the use of capping agents such as ligands, polymers, or surfactants that stabilize the nanoparticle surface through steric and electrostatic interactions, preventing aggregation and providing sufficient size control during synthesis. 1,8,13,14 However, for most applications, the presence of capping agents is detrimental to nanoparticle functionality, causing a variety of problems such as reductions in catalytic activity, 15-20 increased system complexity through charge transfer at the metal-ligand

interface, ²¹ and nonuniform or nonreproducible ligand coverage of the nanoparticle surface. ²¹

Alternatively, recent studies have shown that the use of ionic liquids (ILs) in place of traditional organic or aqueous solvents allows for the preparation of nanoparticles without additional capping agents; the nanoparticles are stabilized via the ionic nature, polarity, and supramolecular network of the IL. 1,22–24 ILs are low melting point salts typically composed of organic cations (e.g., phosphonium, ammonium, pyridinium, and imidazolium) and either organic or inorganic anions (e.g., imides, sulfonates, halides, carboxylates, phosphates). Lis have recently received much attention because of their potential as a "green" and recyclable alternative to traditional organic solvents. ILs offer unique advantages compared to traditional organic and aqueous solvents including high

Received: September 30, 2020 Revised: December 15, 2020 Published: December 30, 2020





polarity, negligible vapor pressure, high solubility, good chemical and thermal stability, and high ionic conductivity. 28-33 Furthermore, IL properties can be tailored to specific applications through different combinations of cations and anions, for example, to favor low viscosity and thermal stability, ^{27,34} to such an extent that ILs haven been dubbed "designer solvents". 35 In recent years, ILs have been intensively studied as new liquid media^{36,37} and specifically for applications in nanoparticle synthesis.^{38–42}

ILs have a fundamental nanostructure configuration, which is a product of their electrostatic interactions, hydrogen bonding, and van der Waals interactions. 43,44 The IL network provides adequate steric and electrostatic stabilization to prevent aggregation and Ostwald ripening through the formation of an ion layer around metallic nanoparticles. 24,45-48 Much research has been dedicated to the synthesis of metallic nanoparticles in ILs through a variety of methods including chemical reductions, 40,41,49-52 photochemical reductions, 39,53 and electroreduction/deposition 54-56 of metallic salts.

Silylamine reversible ionic liquids (RevILs) are a relatively new class of ILs that were originally designed for CO2 sequestration then later repurposed for nanoparticle synthesis.⁵⁷⁻⁶⁰ Silylamine liquids possess a switchable duality capable of converting between the molecular and ionic forms upon reaction with CO₂, according to Scheme 1. RevILs have

Scheme 1. Conversion of Silylamines to RevILs via Reaction with CO₂

properties similar to traditional ILs but also have the advantage of switchable moieties, meaning nanoparticles synthesized with RevILs can be easily stabilized and destabilized at will. Ethier et al. demonstrated that the ionic form of the silvlamine (the RevIL), when combined with a hydrocarbon, functions like a switchable surfactant that can be used to stabilize nanoparticles during synthesis. 57,58 It has been shown previously that RevILs are effective in the synthesis of monodisperse nanoparticles without the use of additional capping agents and that by leveraging the switchable nature of the silylamine, sizecontrolled and highly active nanoparticles can be deposited onto a support material. 61,62 Nanoparticle synthesis in RevIL systems was hypothesized to proceed through a reverse micelle templating mechanism, in which the ion pairs of the IL selfassemble into organized structures possessing an aqueous core. The basis for this hypothesis came from the utilization of methyl orange as a micellar probe molecule. Methyl orange (Figure 1a) is a polar molecule with negligible solubility in hydrocarbon solvents; however, it has been shown that it may become solubilized in a hydrocarbon when supported in micelles.63

Ethier et al. demonstrated the switchable nature of the system by showing that upon mixing of hexane, methyl orange, and a silylamine (3-aminopropyltripropylsilane, TPSA) in its neutral form, as expected, methyl orange did not dissolve into solution because of the nonpolar nature of the mixture. Upon addition of CO₂ and conversion of the TPSA to the ionic form, methyl orange readily dissolved (reproduced results shown in Figure 1b). ⁵⁸ The process could easily be reversed by removal

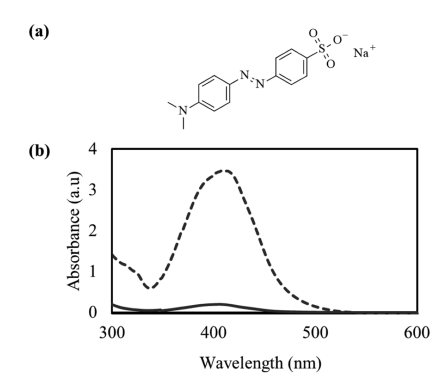


Figure 1. (a) Structure of methyl orange and (b) UV-vis spectra demonstrating the dissolution of methyl orange only upon conversion of the silylamine to ionic form (shown by the dotted line).

of CO2 from the system. From these results, it was hypothesized that the ionic form of TPSA forms organized reverse micelle structures possessing an aqueous core capable of solubilizing the polar methyl orange. Upon reversal of the ionic species to the neutral form, the organized structures disassemble triggering the precipitation of the methyl orange. 51 While the formation of a polar environment capable of solubilizing polar species in a hydrocarbon can be explained by the formation of reverse micelles, it is not direct evidence. Alternative mechanisms such as a cosolvent effect or the formation of IL aggregates without an aqueous core are possible. Silylamine RevILs offer unique and advantageous alternatives to synthesis of dispersed and supported nanoparticles, but the mechanism of nanoparticle synthesis in these systems remains unknown.

In this work, we identify the nanoparticle synthesis mechanism in silylamine RevILs. Here, we use diffusionordered nuclear magnetic resonance (DOSY-NMR) spectroscopy coupled with gold nanoparticle syntheses in an effort to identify the formation of organized structures within the IL synthesis solutions. It is demonstrated that nanoparticle synthesis in RevILs does not proceed through the hypothesized reverse micelle mechanism but rather through a "switchable aggregation" of the ionic silylamine, which affords control over the nanoparticle size through manipulation of the structure and concentration. Furthermore, it is demonstrated that addition of water to RevIL systems is detrimental to the aggregation behavior of the IL molecules.

EXPERIMENTAL SECTION

Materials. Hydrogen tetrachloroaurate tri-hydrate (HAuCl₄·3H₂O; 49% Au), platinum (0)-1,3-divinyl-1,1,3,3tetramethyldisiloxne (Pt-DVDS; ~2% platinum), allylamine $(C_3H_5NH_2; 98)$, and triethylsilane $(C_6H_{16}Si; 99\%)$ were obtained from Sigma-Aldrich. Sodium borohydride (NaBH₄; >97%) and silica (SiO₂; 0.060-0.2 mm) were obtained from Alfa Aesar. Tetramethylsilane (C₄H₁₂Si, >99.9%), bis(2ethylhexyl) sulfosuccinate sodium salt (AOT, C₂₀H₃₇NaO₇S, 96%), and 1-dodecanethiol (C₁₂H₂₆S; 98%) were obtained from Acros Organics. Toluene (C₇H₈; >99.5%), *n*-hexane $(C_6H_{14}; >95\%)$, trisodium citrate $(Na_3C_6H_5O_7; >99\%)$, and hydrochloric acid (HCl; 36.5-38%) were obtained from J.T. Baker. Trihexylsilane (C₁₈H₄₀Si, >95%) was purchased from TCI. Deuterated benzene (C₆D₆, 99.5%) was purchased from Cambridge Isotope Laboratories, Inc. Clinical laboratory reagent water-Type 1 was obtained from Thermo Fisher Scientific. 200 mesh Carbon/Formvar-coated copper grids were purchased from Ted Pella. Toluene was dried over molecular sieves for at least 24 h prior to use. All other materials were used without further purification.

Synthesis of 3-Aminopropyltriethylsilane and 3-Aminopropyltrihexylsilane RevILs. The molecular (i.e., nonionic) silylamines 3-aminopropyltriethylsilane (APTES) and 3-aminopropyltrihexylsilane (APTHS) are not commercially available and were synthesized following a procedure published in the literature.⁵⁷ The silylamines were synthesized through a one-step hydrosilylation reaction. 160 mmol of the silane of interest was mixed with 1.6 mmol of Pt-DVDS in a sealed flask under a nitrogen atmosphere. 320 mmol of allylamine and 80 mL of toluene were then added to the flask while stirring at 300 rpm. The contents of the flask were heated to ~110 °C and the reaction proceeded under refluxing toluene for 24 h. Synthesis of the desired silylamine was verified using ¹H NMR on a Varian VNMRS 600. The APTES and APTHS synthesis products were purified via vacuum distillation at ~65 °C and 2 Torr, and ~165 °C and 2 torr, respectively. The purified silylamines were stored under dry nitrogen at room temperature prior to use.

The APTES and APTHS RevIL were prepared by sparging the molecular silylamines with CO₂. Sparging continued until no mass change was identified in the ILs for three consecutive measurements indicating complete conversion.

RevIL Synthesis of Gold Nanoparticles. Gold nanoparticles were synthesized under various conditions by manipulating the structure of the RevIL (APTES or APTHS), the concentration of the RevIL, or the concentration of added water. For every synthesis, the molecular amine (0.5 mL of APTES or 1.0 mL of APTHS) was added to a sealed, nitrogen-purged vial. CO2 was sparged through the molecular liquid as described above to form the RevIL. HAuCl₄ and hexane were then added to create solutions of the desired concentration while ensuring equal gold-to-IL ratios within each experiment. The mixtures were sonicated until the HAuCl₄ had completely dissolved. For experiments investigating the impacts of added water, aliquots of water were added to reach the desired concentrations and again sonicated. The nanoparticles were then reduced via rapid addition of aqueous NaBH₄ while stirring at 400 rpm. While the volume of aqueous NaBH₄ added varied depending on the experiment (and concentration of the prepared NaBH₄), the molar ratio of Au/ NaBH₄ was maintained at approximately 1.7 in every synthesis.

Transmission Electron Microscopy. The as-synthesized, dispersed nanoparticles were diluted in hexane, then drop-cast on to 200 mesh carbon/Formvar copper grids. TEM micrographs were obtained using a FEI Tecnai G2 T20 Twin TEM operating at a voltage of 200 kV. Image analysis was performed with ImageJ software and at least 300 nanoparticles were manually sized (along the largest particle axis) to ensure statistical significance.

¹H and ¹³C NMR. All ¹H and ¹³C NMR experiments were conducted on a Varian VNMRS 600 and 500 MHz nuclear magnetic resonance spectrometers, respectively. All samples were equilibrated in the magnet for 30 min prior to spectra acquisition at 298 K. Spectra were collected using standard pulse sequences provided by Varian. 64 transients were analyzed for each ¹H spectrum and 512 variants for each ¹³C spectrum. The chemical shifts of all species were referenced with respect to the benzene peak at 7.33 ppm (128 ppm for ¹³C) or tetramethylsilane (TMS). Peak assignments for the

APTHS IL are very similar to the APTES IL with additional overlapping CH₂ peaks associated with the longer alkyl chain. Peak assignments for the molecular APTES are as follows: [1HNMR (600 MHz, C_6D_6): δ (ppm): 2.65 (t, 2H, -CH₂- NH_2), 1.43 (m, 2H, $-CH_2-CH_2-CH_2$), 1.11 (t, 9H, $-CH_2-CH_2$) $\underline{CH_3}$), 0.81 (s, 2H, $-\underline{NH_2}$), 0.65 (q, 6H, $-\underline{CH_2}$ -Si), 0.58 (t, 2H, $-CH_2-CH_2-CH_2-NH_2$]. Peak assignments for the APTES RevIL are: [1 HNMR (600 MHz, $C_{6}D_{6}$): δ (ppm): 9.13 $(s, 3H, -NH_3^+), 5.22 (s, 1H, -CH_2-NH-C-), 3.35 (t, 2H,$ $-CH_2-CH_2-NH_3^+$), 2.90 (t, 2H, CH_2-CH_2-NH-), 1.86 $(m, 2H, -\underline{CH}_2-CH_2-NH_3^+), 1.63 (m, 2H, -\underline{CH}_2-CH_2-$ NH-), 1.10 (t, 18H, -CH₂-<u>CH₃</u>), 0.66 (t,12H, CH₃- $\underline{CH_2}$ -). 0.60 (t, 4H, -Si- $\underline{CH_2}$ - $\overline{CH_2}$)]. ¹³C peak assignments for APTES RevIL with and without HAuCl₄ present are: [13 CNMR (500 MHz, C_6D_6): δ (ppm): 163.3 (1C, $-\underline{C}O_2^-$), 45.7 (1C, $-\underline{C}H_2-NH-$), 43.2 (1C, $-\underline{C}H_2-NH_3^+$), 25.4 $(-\underline{C}H_2-CH_2-NH-)$, 23.2 (1C, $-\underline{C}H_2-CH_2-NH_3^+$), 9.0 $(1C, -\underline{C}H_2-CH_2-CH_2-NH_3^+), 7.7 (1C, -\underline{C}H_2-CH_2 CH_2-NH-$), 3.7 (12C, $-\underline{C}H_2-Si-$ and $\underline{C}H_3-CH_2-$). Peak assignments for dioctyl sulfosuccinate sodium salt (AOT) are as follows: [1HNMR (600 MHz, C_6D_6): δ (ppm): 4.60 (dd, 1H, O_3 -S- \underline{CH}), 4.35 (m, 2H, O_3 -S- \underline{CH} - \underline{CO}_2 - \underline{CH}_2), 4.30 (m, 2H, O_3 -S-CH-CH₂-CO₂- $\frac{CH_2}{}$), 3.60 (m, 2H, O_3 -S- $CH - \underline{CH_2} - CO_2$), 2.00 (m, 2H, $CH - (\underline{CH_2})_3$), 1.53 (m, 16H, $\underline{CH}_2 - \underline{CH}_3$), 1.18 (m, 12H, $-\underline{CH}_2 - \underline{CH}_3$)].

¹H Diffusion-Ordered NMR Spectroscopy. ¹H DOSY spectra were collected utilizing a bipolar pulse pair-stimulated echo with a convection compensation sequence provided by Varian (Dbppste_cc). All spectra were collected at 298 K. The length of the diffusion-encoding gradient was varied as a function of sample viscosity from 0.4 ms for low viscosity samples to 2.5 ms for high viscosity samples. The d-1 delay between each experiment was 2 s, the diffusion delay was set to 200 ms, and the grad-90-grad pulse sequence was enabled. The amplitude of the diffusion gradient was varied linearly in 16 increments ranging from 2.96 and 59.91 G·cm⁻¹. At least eight transients were used to produce each sample. The diffusion coefficient of the molecular amine was calculated with the peak integral of the -CH₂- in the alpha position to the amine (Figure 2a). Diffusion coefficients of the APTES and APTHS IL samples were calculated using the peak integral of -CH₂-

(a)
$$NH_2$$

(b) $NH_3^+ - O NH_3^+ - O NH_3$

Figure 2. Structures of (a) molecular APTES, (b) APTES RevIL, and (c) APTHS RevIL.

in the alpha position to the carbamate (Figure 2b,c). Diffusion calculations in VNMRJ (v4.2) were performed using the modified spline model (SPLMOD) including a correction for nonuniform gradients.

NMR Sample Solutions. AOT Reverse Micelle Solution. A 180 mM solution of AOT was prepared in deuterated benzene in a 1 mL volumetric flask. The solution was thoroughly mixed via sonication prior to the addition of water resulting in a water-to-surfactant ratio of 10. The sample was then transferred to an NMR tube and a capillary containing TMS and deuterated benzene was inserted at the center.

Silvlamine Solutions. Silvlamine solutions were prepared under various conditions for ¹H and DOSY-NMR analyses. The variables manipulated for DOSY experiments include concentrations of molecular APTES (0.1-5.3 M), concentrations of ionic APTES (0.001-2.36 M) and ionic APTHS (0.05-1.22 M), structure of the IL (APTES vs APTHS), the presence of gold precursor (0-28 mM), and concentration of added water (0.1-5.0 M). For all DOSY experiments, the samples were dissolved in hexane to prepare the desired concentrations. The variables manipulated for standard ¹H NMR were concentration of added water and concentration of added protons in APTES IL/hexane solutions. All samples were prepared in 1 ml volumetric flasks. For all DOSY experiments, the lock solvent (deuterated benzene) was placed in a capillary and inserted into the NMR tube containing the sample solution. Each sample was scanned twice: once with TMS in the capillary and once with TMS in the sample solution such that TMS could be used as an internal viscosity standard. Standard ¹H NMR was used to determine the effect of added water and added protons on chemical shift values; water was varied from 0 to 1.3 M and protons were added with either HAuCl₄ (0.0100 g) or HCl (2.12 µL) such that the concentration of added protons in each sample was equal. For all solutions prepared for standard ¹H NMR, the lock solvent (deuterated benzene) was used as the sample solvent. For all samples containing the gold precursor, the Au/IL ratio was held constant and all samples containing gold precursor or water were aged 24 h prior to analysis.

■ RESULTS AND DISCUSSION

Previous work demonstrated the use of silvlamine RevILs for the synthesis and deposition of size-controlled nanoparticles. \$8,61,62 A typical nanoparticle synthesis in these systems starts with the dissolution of a metallic precursor in a RevIL and hexane solution followed by reduction via addition of aqueous NaBH₄. It was hypothesized that nanoparticle formation followed a reverse micelle mechanism, in which nanoparticles were stabilized and templated within the aqueous core of the organized structure. In reverse micelle synthesis mechanisms, the size of the aqueous micellar core and the resulting nanoparticle size are directly dependent on a variety of factors including the solvent used, 64 the concentration of reagents,65 the structure of the surfactant molecule,66,67 and the water-to-surfactant ratio $(W_0)^{.68,69}$ In this work, the surfactant structure and water-to-surfactant ratio were leveraged to attempt to identify reverse micelle structures in RevIL nanoparticle synthesis solutions. A combination of standard ¹H NMR, DOSY-NMR, and nanoparticle syntheses was used to determine the effects of W_0 and IL structure on behavior of the IL in solution and resulting nanoparticle size.

Identification of an Aqueous Micellar Core with ¹H NMR. Reverse micelles with cores of water should exhibit bulk-

water signals (i.e., the formation of water—water hydrogen bonds) in the 1 H spectra. To validate the 1 H NMR technique for detection of an aqueous micellar core, experiments were first performed using AOT, a control molecule well known to form reverse micelles in solution. Standard 1 H NMR scans were performed on AOT and APTES IL solutions to detect the presence of bulk water. Previous work has shown that the chemical shift of bulk water in AOT reverse micelles is dependent upon the structure of surfactant molecule as well as the solvent used. Under the conditions tested (180 mM AOT and $W_{\rm o}=10$), the chemical shift of bulk water in the core the of reverse micelle should appear near 4.80 ppm. Figure 3a shows the presence of bulk water at 4.81 ppm in the

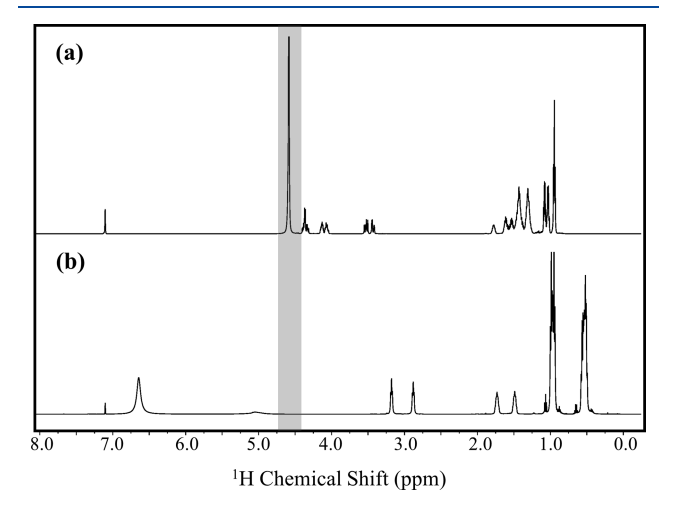


Figure 3. ¹H NMR spectra of (a) AOT in benzene- d_6 reverse micelles (b) APTES RevIL in benzene- d_6 at the same concentration of added water ($W_0 = 10$).

AOT sample as expected for reverse micelle solutions. However, no peak that can be associated with bulk water is seen in the APTES spectrum (Figure 3b) at the same concentration of water ($W_{\rm o}=10$). The absence of bulk water in the APTES sample indicates that there are no aqueous micellar cores present.

DOSY-NMR Analysis. Although an aqueous core was not detected in the APTES RevIL samples using standard ¹H NMR, DOSY-NMR was used to determine the effect of water addition on the diffusion of the IL molecules. If reverse micelles are present in solution, the addition of water would result in swelling of the micellar core, ultimately reducing the diffusion coefficient of the species. DOSY-NMR allows for the determination of diffusion coefficients (and hydrodynamic radii) of components in a mixture by leveraging spatially dependent magnetic field gradients coupled with radio-frequency pulses. Diffusion coefficients were calculated using the Stejskal—Tanner equation (eq 1)⁷¹ based on the extent of signal attenuation resulting from translational diffusion along the applied magnetic field gradient.

$$\ln\left(\frac{I}{I_o}\right) = -D\gamma^2 G^2 \delta^2 \left(\Delta - \frac{\delta}{3}\right) \tag{1}$$

Here, I and $I_{\rm o}$ are the observed signal and the signal amplitude prior to an applied gradient pulse, respectively, D is the measured diffusion coefficient, γ is the gyromagnetic ratio of the nucleus of interest, G is the strength of the applied magnetic field gradient, δ is the duration of the applied pulse,

and Δ is the length of the diffusion delay. Diffusivity measurements were then used to calculate hydrodynamic radii of each species of interest using the Stokes–Einstein relation (eq 2). Diffusion coefficients were referenced to the diffusivity of a spherical, noninteracting molecule (TMS), which functioned as an internal viscosity standard.

$$\frac{D_{\rm i}}{D_{\rm st}} = \frac{\frac{k_{\rm B}T}{c_{\rm i}\pi\eta R_{\rm i}}}{\frac{k_{\rm B}T}{c_{\rm st}\pi\eta R_{\rm st}}} = \frac{c_{\rm st}R_{\rm st}}{c_{\rm i}R_{\rm i}}$$
(2)

Here, $D_{\rm i}$ and $D_{\rm st}$ are diffusion coefficients of the species of interest and the standard, respectively, $k_{\rm B}$ is Boltzmann's constant, T is the absolute temperature, η is the solvent viscosity, $R_{\rm i}$ and $R_{\rm st}$ are the hydrodynamic radii of the species of interest and the standard, respectively, and c is a shape correction factor to account for nonspherical sample molecules and is calculated empirically (eq 3).

$$c_{i} = \frac{6}{1 + 0.695 \left(\frac{R_{\text{solvent}}}{R_{i}}\right)^{2.234}}$$
(3)

This DOSY pulse sequence has been validated previously for the identification of reverse micelles using AOT. An increase in water loading is known to increase the aqueous core size of AOT reverse micelles. It was shown that as the water-to-surfactant ratio increased, the calculated hydrodynamic radius $(R_{\rm H})$ of the surfactant also increased. The calculated values of $R_{\rm H}$ were comparable to those obtained by dynamic light scattering, demonstrating the ability to detect reverse micelles using this DOSY pulse sequence and data analysis method.

Effect of W_o on R_H of APTES IL. The water-to-surfactant ratio was varied in a 1.5 M solution of APTES IL in hexane then analyzed with DOSY-NMR in order to detect micellar core swelling indicative of reverse micelles. A typical DOSY-NMR spectrum is shown in Figure 4. Because of the low volume of the deuterated solvent used (only in a capillary), the relative size of the peak associated with residual benzene is small and not seen at this scale. The measured diffusion coefficients of the IL molecules at each W_o tested were

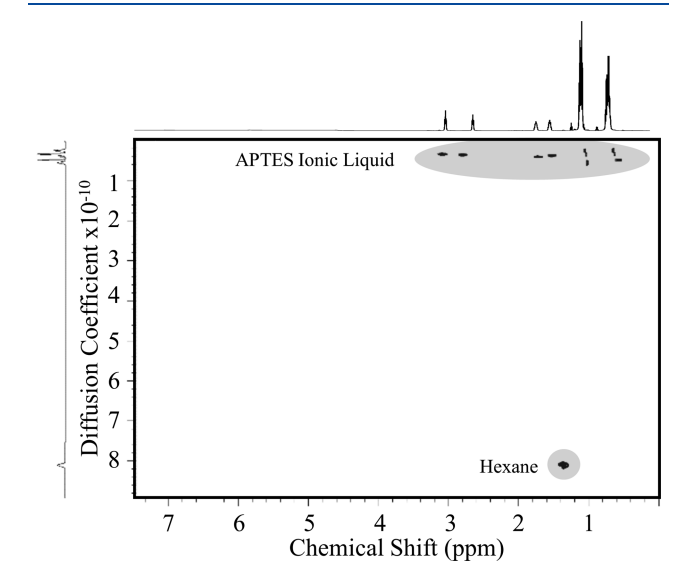


Figure 4. Typical DOSY-NMR output of APTES IL in hexane with no added water.

determined to be 1.57×10^{-10} , 1.56×10^{-10} , 1.59×10^{-10} , and 1.59×10^{-10} m²/s. Hydrodynamic radii, calculated using eqs 2 and 3, were 4.46, 4.53, 4.45, and 4.50 nm for $W_o = 0.04$, 0.4, 1.3, and 2.1, respectively. These results imply that increased water loading does not increase the hydrodynamic radius of the IL. Given that no bulk water core exists and that there is no increase in size upon the addition of water, it can be concluded that the nanoparticle synthesis does not occur through a reverse micelle process.

Effect of W_0 on Nanoparticle Size. In reverse micelle nanoparticle syntheses, it is well documented that increasing W_0 (prior to reduction) not only increases the size of the aqueous micellar core, but also increases the size of the resulting nanoparticles. 66,68,75 In most cases, the size of the reverse micelle structures varies linearly with W_0 . 69 While the aqueous micellar core functions as a template for nanoparticle synthesis, the size of the resulting nanoparticles is typically smaller than the size of the aqueous core by roughly an order of magnitude. 65 Because it was found that R_H of the APTES IL does not change in response to W_0 , the size of the resulting nanoparticles was similarly expected to remain constant. Nanoparticles were synthesized using APTES IL solutions by varying W_0 prior to the reduction in each synthesis. Water concentration was varied (at constant IL concentration) from 0.6 to 5.8 M. TEM micrographs of the resulting nanoparticles are shown in Figure 5. As expected, the nanoparticle size is not statistically different under any of the synthesis conditions tested (as determined by a single-factor ANOVA analysis and Tukey HSD^{76} with p < 0.01). Combining the results of the nanoparticle syntheses with the ¹H and DOSY-NMR studies above, it is clear that nanoparticle synthesis in RevIL systems does not occur through the hypothesized reverse micelle mechanism.

Effects of Concentration and Structure on Molecular Aggregation. Because it was found that nanoparticle synthesis does not proceed through a reverse micelle mechanism, additional DOSY studies were performed in an effort to identify how the ILs behave in solution prior to the addition of the metallic precursor and reducing agent. Previous work studying the nanoparticle synthesis mechanism using the Brust-Schiffrin method demonstrated that tetraoctylammonium bromide (TOA-Br) ions, which were hypothesized to form reverse micelles in solution, actually formed ion-ion aggregates where the increase in $R_{\rm H}$ with increasing $W_{\rm o}$ was attributed to hydration of the anion rather than the formation of an aqueous micellar core. 70 Furthermore, it was demonstrated that the extent of the ion-ion aggregation was a function of TOA-Br concentration in solution, such that the size of the aggregates increased with concentration, ultimately resulting in an increase in the nanoparticle size. In this work, similar experiments were performed to identify the aggregation behavior of the silylamines in solution.

Figure 6 shows $R_{\rm H}$ calculated as a function of silylamine concentration in hexane. Here, it is shown that as the concentration of the APTES IL is increased from 0.0010 to 2.4 M, $R_{\rm H}$ increases from 0.22 to 56 nm, respectively, indicating the formation of large IL aggregates in solution. Similarly, when the size of the IL molecules is increased from APTES to APTHS at 1 M concentration, the $R_{\rm H}$ increases from 2.6 to 11 nm. These results demonstrate the degree of aggregation is directly dependent on both the structure and concentration of the IL molecules. While some aggregation is seen in the molecular APTES sample, it is only observed at very high

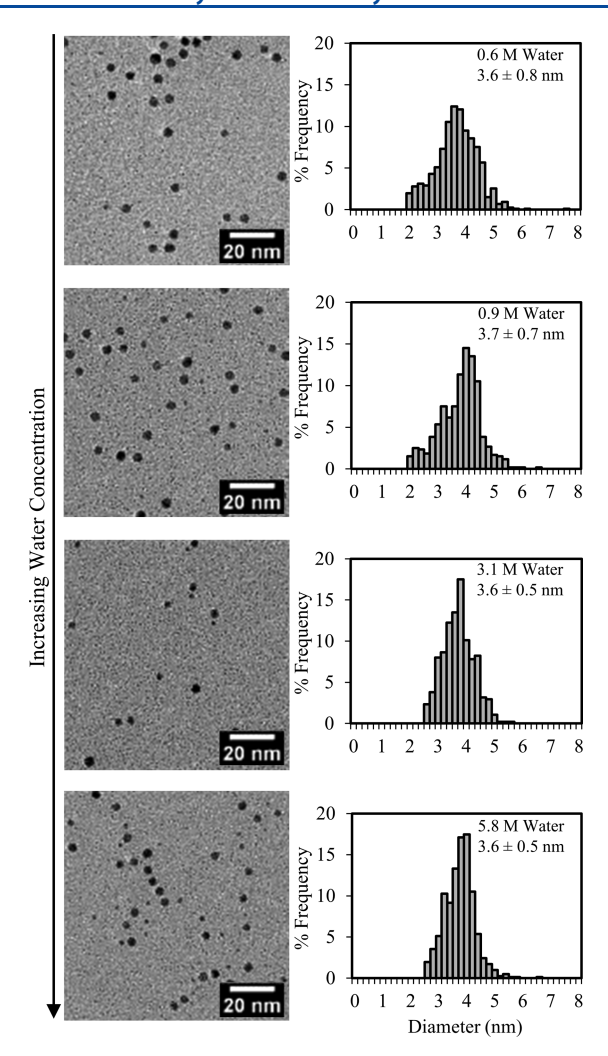


Figure 5. TEM micrographs and size distributions of Au nanoparticles synthesized with APTES in increasing water concentration.

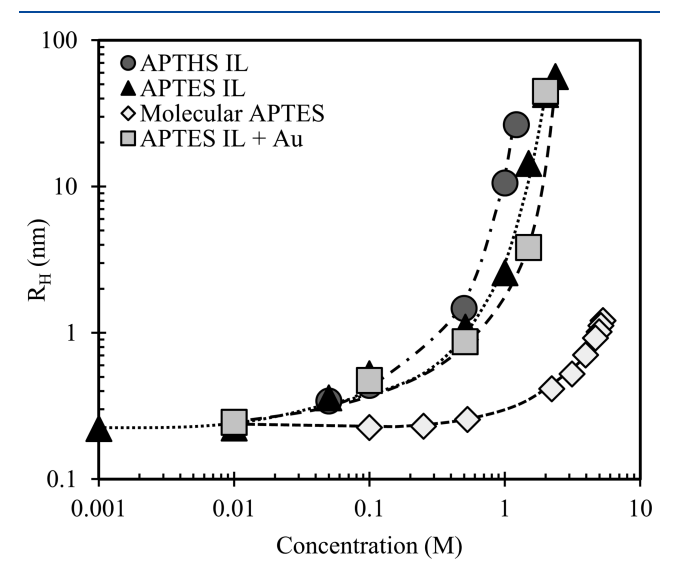


Figure 6. Calculated hydrodynamic radii of silylamines at various concentrations. Dashed lines are to guide the eyes.

concentrations and not nearly to the extent of the IL samples. Additionally, when the gold precursor HAuCl₄ is added to the APTES IL solutions, only negligible differences are seen in the

aggregation of the ionic species, demonstrating that under nanoparticle synthesis conditions (0.51 M IL and 3.0 mM $HAuCl_4 \cdot 3H_2O$) the IL behaves in the same manner.

Speciation in RevIL Nanoparticle Synthesis Solutions. While DOSY experiments showed aggregation of ILs in synthesis solutions with and without the metallic precursor, these results do not indicate where nanoparticle synthesis takes place. If nanoparticle synthesis occurs within the RevIL aggregates, these assemblies would likely function as a template or a microreactor, resulting in changes in the nanoparticle size with changes in the aggregate size. ¹H NMR was used to determine if gold nanoparticle synthesis in silylamine systems occurs within the IL aggregates, whereby the RevIL acts as a chelator for the gold ions. Here, three solutions of 0.51 M APTES IL were prepared. The first sample acted as a control with no added protons (Figure 7a). To a second sample, the

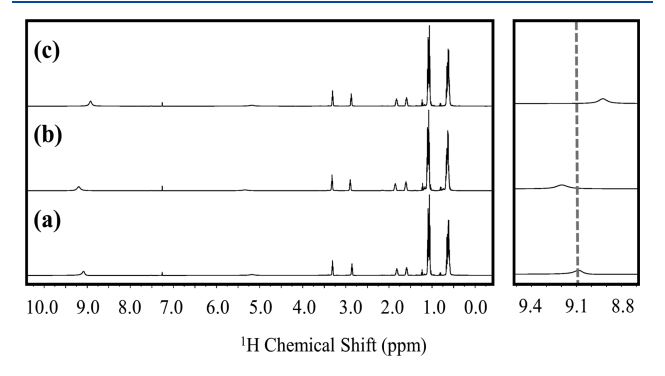


Figure 7. ¹H NMR spectra of (a) APTES RevIL control, (b) APTES RevIL and HAuCl₄, and (c) APTES RevIL and HCl.

gold precursor, HAuCl₄, was added (Figure 7b). A downfield shift was detected in the peak associated with NH₃⁺ of the IL from 9.08 ppm in the control sample to 9.20 ppm in the sample containing HAuCl₄. This downfield shift is the result of deshielding of the NH₃⁺ protons by the AuCl₄⁻ species of the gold precursor. To eliminate potential effects of the addition of the acidic proton, HCl was added to a third sample for comparison (Figure 7c). The sample containing HCl shows a slight upfield shift of the NH₃⁺ peak from 9.08 ppm in the control sample to 8.92 ppm. This upfield shift is because of the shielding effect of the acidic protons. These results demonstrate that the shift observed after HAuCl₄ addition is not because of the presence of acid protons, but rather because of the presence of the AuCl₄ species near the ammonium groups of the IL. The interaction between the gold precursor and the IL molecules is an indication that local high concentrations of the metallic precursor exist within the IL aggregates prior to reduction during nanoparticle synthesis.

Impacts of Water on IL Aggregation. While it was shown previously that water addition has little influence on the size of the synthesized nanoparticles under the tested conditions, when 1 M water (standard nanoparticle synthesis concentration) and 5 M are added to the solutions of increasing IL concentration, the hydrodynamic radii of APTES are significantly lower than in the absence of water but are maintained at roughly 4.5 nm for both water additions (Figure 8). The maintenance of hydrodynamic radius even as the water concentration increases indicates that the disassembly of the IL networks tends toward a thermodynamic minimum. This phenomenon was observed at concentrations as low as 0.1 M added water (not shown). When no water is added to the

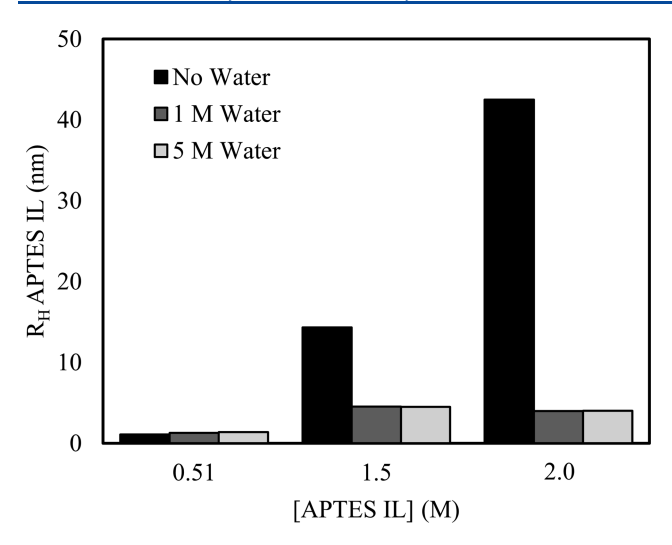


Figure 8. Calculated hydrodynamic radii of APTES RevIL solutions of various water and IL concentrations.

system, the IL aggregates as previously shown (i.e., as the IL concentration increases, larger aggregates form). Additionally, when 0.009 M water is added to the IL systems in the form of complexed water in $HAuCl_4 \cdot 3H_2O$, the aggregation remains unaffected as shown in Figure 6, above.

This separating effect of water on the ion pairs has been shown previously in the case of protic ILs. This phenomenon can be explained by the complexation of the ammonium ions of the IL with the hydroxide ions of the added water, instead of the intended carbamate ions of the IL. This implies that during nanoparticle synthesis, prior to addition of water (with NaBH₄), the gold precursor is stabilized by the ammonium ions, which are near the carbamate ions of the IL, resulting in large aggregates. There is no indication of an interaction between the carbamate ions and gold chloride ions in the ¹³C NMR spectra (no difference in chemical shift), indicating that prior to reduction, the gold precursor interacts primarily with the ammonium ions. However, after reduction (i.e., addition of aqueous NaBH₄) the aggregates disassemble as a result of ammonium complexation with hydroxide ions and the nanoparticles become stabilized only by the carbamate ions (as previously demonstrated with FTIR⁶⁴). Because it was previously shown that water addition has no effect on the nanoparticle size, this implies that the disassembly of the ammonium-carbamate ion pairs is slower than the reduction of the nanoparticles stabilized within the aggregates.

The ¹H NMR spectra in Figure 9a—e show that as the concentration of added water is increased, there is a significant upfield shift in the peak associated with the NH₃⁺ of the IL. The peak associated with the ammonium protons shifts from 9.13 ppm in the RevIL sample containing no water (Figure 9a) to 7.01 ppm in the sample containing 1.3 M added water (Figure 9e). This is likely because of the rapid exchange of the ammonium protons with water protons, causing a larger shift (to lower chemical shift values) as more protons from added water become available for exchange.

Effects of IL Aggregation on Nanoparticle Size. To better understand how IL aggregation impacts the resulting nanoparticle size, nanoparticles were synthesized in APTES and APTHS at various concentrations. TEM micrographs and average diameters are shown in Figure 10a-d. Nanoparticles synthesized at low IL concentration (0.05 M APTES) (Figure

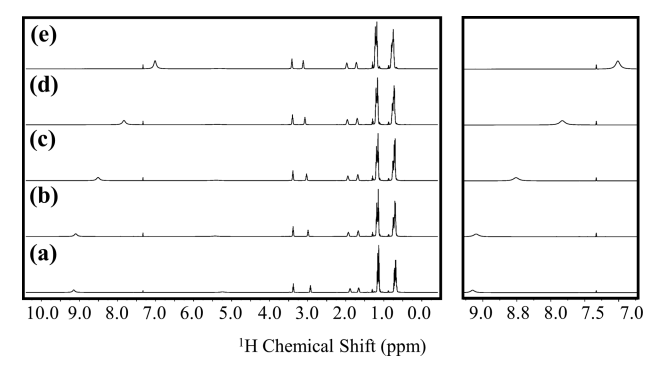


Figure 9. ¹H NMR spectra of APTES RevIL with increasing concentrations of added water (a) APTES RevIL control, (b) 0.089, (c) 0.22, (d) 0.44, and (e) 1.3 M.

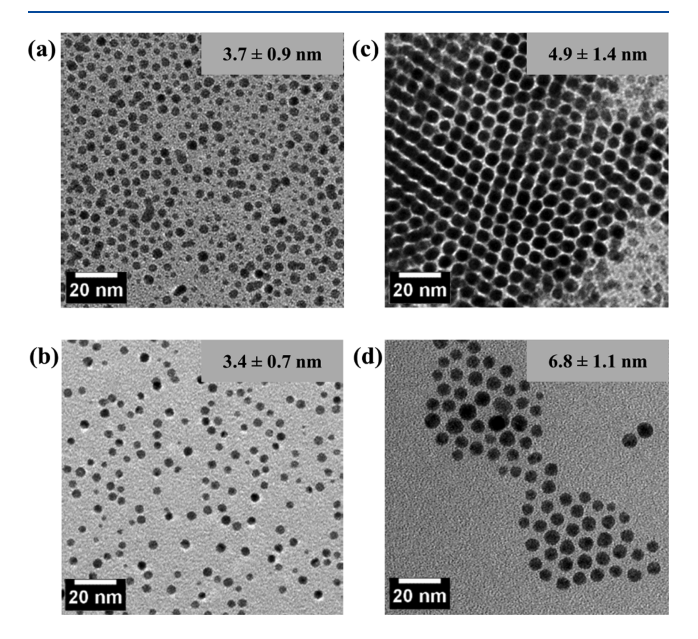
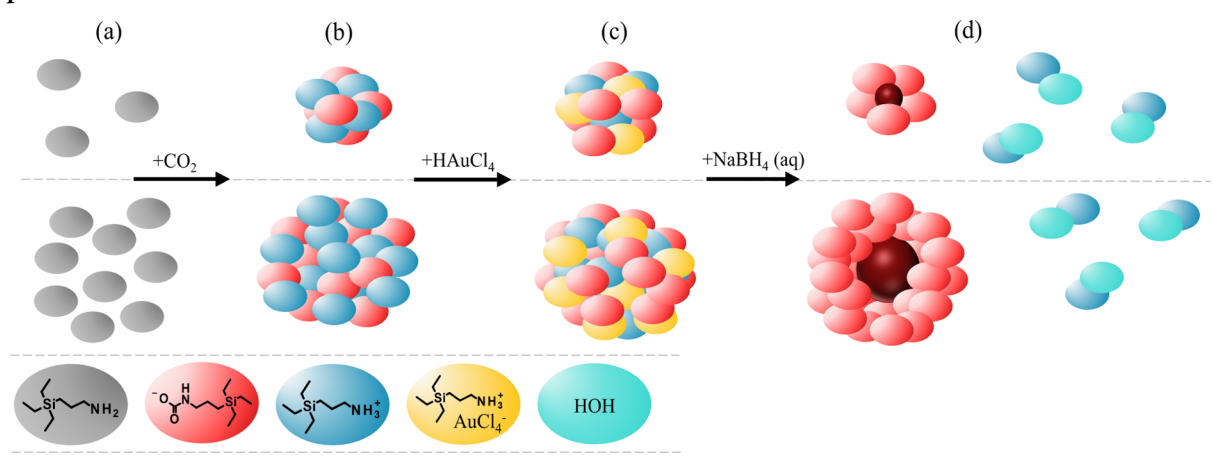


Figure 10. TEM micrographs and average diameters of nanoparticles synthesized with (a) 0.05 M APTES RevIL, (b) 0.51 M APTES RevIL, (c) 1.5 M APTES RevIL, and (d) 0.5 M APTHS RevIL.

10a) are not statistically different in size compared to those synthesized at standard IL synthesis concentrations (0.51 M), shown in Figure 10b. However, a significant size increase is seen in nanoparticles synthesized at high RevIL concentration (1.5 M APTES) increasing from 3.4 ± 0.7 nm under standard conditions to 4.9 ± 1.4 nm at high concentrations as seen in Figure 10c. Similarly, as the RevIL structure size increases from APTES to APTHS at standard IL concentration (0.51 M), the nanoparticle size is again significantly increased from 3.4 ± 0.7 to 6.8 ± 1.1 nm (Figure 10d). These results demonstrate that the nanoparticle size is directly dependent on both the concentration and structure of the IL and thus, the size of the IL aggregates. While it has been shown that nanoparticle formation does not proceed through a reverse micelle mechanism, here it is shown that synthesis in RevIL systems occurs through a "switchable aggregation" mechanism, whereby the RevIL molecules reversibly form aggregates without an aqueous core upon reaction with CO2 affording control over the nanoparticle size. It has been demonstrated in a previous work that the RevIL aggregates can be disassembled at will upon removal of CO₂ in order to facilitate the destabilization of nanoparticles for deposition on to a surface. 61,62 A schematic

Scheme 2. Hypothesized RevIL Switchable Aggregation Nanoparticle Synthesis Mechanism; (a) Neutral Silylamine Reacts with CO₂ to Form the RevIL; (b) RevIL Aggregates Form Where the Size of the Aggregate Depends on Concentration and Structure of the IL Molecules; (c) Anionic Gold Salt is Sequestered within the RevIL Aggregates, Stabilized Primarily by the Ammonium Ions; (d) Addition of the Aqueous Reducing Agent Results in the Formation of Gold Nanoparticles and Subsequent Dissociation of the RevIL Ion Pairs



of the hypothesized nanoparticle synthesis mechanism is shown in Scheme 2. While more investigation is needed, it appears that there exist optimal conditions (such as those used in Figure 10c) to synthesize large populations of highly monodisperse nanoparticles (likely because of better capping of the nanoparticles at high RevIL concentration), demonstrating that size and polydispersity are tunable in these systems. Further investigation is needed to determine the achievable maximum nanoparticle size using this method; however, it is hypothesized that further increasing the size of the RevIL will increase the size of synthesized nanoparticles because of the formation of larger aggregate domains.

In both cases, populations of highly monodisperse nanoparticles are formed as a result of the high RevIL concentrations, leading to better stabilization by the carbamate ions. However, the size of the nanoparticles significantly decreases from 4.9 ± 1.4 nm with no water prior to reduction (Figure 10c) to 3.2 ± 0.9 nm when water is present prior to reduction (Figure 11).

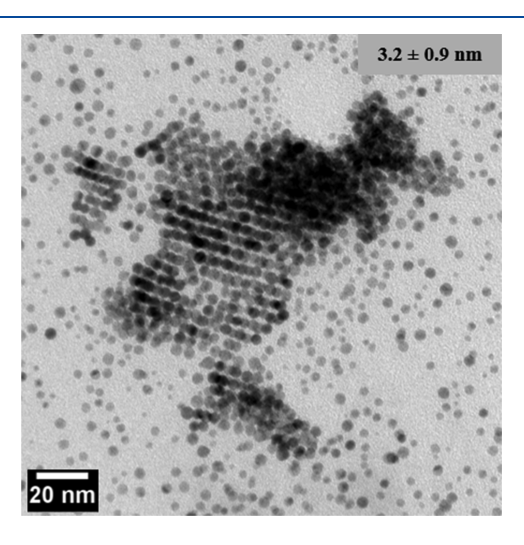


Figure 11. TEM micrograph and average diameter of nanoparticles synthesized in 1.5 M APTES and 5 M water added prior to reduction.

From these results, we can confirm that water added prior to reduction serves to reduce aggregate domains via disassembly of the ion pairs of the RevIL. However, in the case of the "standard" synthesis (0.51 M RevIL), the presence of water does not impact the final nanoparticle size. This is because the aggregate domains, while smaller, are likely equivalent to a homogeneous distribution of gold ions, that is, local gold ion concentration does not change with changing domain size resulting from water addition. If local concentration of gold ions does not change within the aggregate domains, a change in the nanoparticle size would not be expected (as is shown above). While more investigation is needed, these results also suggest that further reducing the size of the RevIL (smaller than APTES RevIL) will likely not result in a significant decrease in the nanoparticle size.

In the case of larger aggregate domains resulting from the high (1.5 M) RevIL concentration (and no water), the system is further from a homogeneous distribution (i.e., further away from infinite dilution) of the gold ions, resulting in the formation of larger nanoparticles because of the higher local concentrations of gold ions. When water is added to this system, aggregate domains are reduced in size, causing a decrease in the local concentration of gold ions within the aggregates available for nanoparticle growth and ultimately resulting in smaller nanoparticles.

Conclusions. It was previously demonstrated that the use of silylamine RevILs offers an advantageous alternative to traditional nanoparticle synthesis techniques. However, until now, the mechanism of nanoparticle synthesis in these systems remained poorly characterized. Here, it was shown that synthesis in RevIL systems does not proceed through the previously hypothesized reverse micelle mechanism, but rather through a switchable aggregation mechanism. Results of DOSY experiments show that when the RevIL is combined with an alkane solvent, large IL aggregates assemble in solution. Addition of the gold precursor to this solution leads to high local concentrations of the gold ions within the large IL aggregates, whereby the aggregates create regions that behave as microreactors. Upon addition of the aqueous reducing agent, classical nanoparticle nucleation and growth proceeds (where larger aggregates have higher gold concentration and

lead to larger nanoparticles) as well as the water-driven disassembly of the IL aggregates. However, it was shown that nanoparticle size remains relatively unaffected by the addition of water, implying that nanoparticle nucleation and growth must occur faster than the disassembly process. Furthermore, it was demonstrated there is a direct correlation between the nanoparticle size and structure and concentration of the RevIL ultimately allowing for control over the nanoparticle size and monodispersity in these systems. While in-depth studies of other metals have not yet been completed, preliminary work has shown that platinum, palladium, and silver nanoparticles can be prepared using APTES RevIL suggesting that RevILs function in a similar manner in a variety of metallic systems.

In this work, it was demonstrated how understanding the mechanism of nanoparticle synthesis in SwiS systems directly led to the ability to tune nanoparticle size, an essential step in the precise tailoring of nanoparticles to specific applications. This work provides understanding of synthesis mechanisms not only in RevIL systems, but potentially traditional IL systems as well and further highlights the importance of elucidating nanoparticle synthesis mechanisms for applications that require fine control over the particle size.

AUTHOR INFORMATION

Corresponding Author

Steven R. Saunders — The Gene and Linda Voiland School of Chemical Engineering and Bioengineering, Washington State University, Pullman, Washington 99164, United States; Department of Chemistry, Washington State University, Pullman, Washington 99164, United States; orcid.org/0000-0001-6714-7435; Phone: 509-335-6578; Email: steven.r.saunders@wsu.edu

Authors

Kristin Bryant — The Gene and Linda Voiland School of Chemical Engineering and Bioengineering, Washington State University, Pullman, Washington 99164, United States

Ellis Hammond-Pereira — The Gene and Linda Voiland School of Chemical Engineering and Bioengineering, Washington State University, Pullman, Washington 99164, United States

Complete contact information is available at: https://pubs.acs.org/10.1021/acs.jpcb.0c08908

Author Contributions

The manuscript was written through the contributions of all authors. All authors have given approval to the final version of the manuscript.

Funding

This work was supported by the National Science Foundation under CBET-1651597 and institutional funding from Washington State University.

Notes

The authors declare no competing financial interest.

ACKNOWLEDGMENTS

The authors thank the Franceschi Microscopy & Imaging Center and the NMR facility at Washington State University. The WSU NMR Center equipment is supported by NIH grants RR0631401 and RR12948, NSF grants CHE-9115282 and DBI-9604689, the Murdock Charitable Trust, and private donors Don and Marianna Matteson.

REFERENCES

- (1) Bönnemann, H.; Richards, R. M. Nanoscopic Metal Particles Synthetic Methods and Potential Applications. *Eur. J. Inorg. Chem.* **2001**, 2455–2480.
- (2) Magnetic Nanoparticles: From Fabrication to Clinical Applications; Thanh, N. T. K., Ed.; CRC Press: Boca Raton, 2012.
- (3) Pankhurst, Q. A.; Thanh, N. T. K.; Jones, S. K.; Dobson, J. Progress in Applications of Magnetic Nanoparticles in Biomedicine. *J. Phys. D: Appl. Phys.* **2009**, *42*, 224001–224016.
- (4) Hyeon, T. Chemical Synthesis of Magnetic Nanoparticles. *Chem. Commun.* **2003**, 927–934.
- (5) Atwater, H. A.; Polman, A. Plasmonics for Improved Photovoltaic Devices. *Nat. Mater.* **2010**, *9*, 205–213.
- (6) Sozer, N.; Kokini, J. L. Nanotechnology and Its Applications in the Food Sector. *Trends Biotechnol.* **2009**, 27, 82–89.
- (7) Narayanan, R.; El-Sayed, M. A. Catalysis with Transition Metal Nanoparticles in Colloidal Solution: Nanoparticle Shape Dependence and Stability. *J. Phys. Chem. B* **2005**, *109*, 12663–12676.
- (8) Astruc, D.; Lu, F.; Aranzaes, J. R. Nanoparticles as Recyclable Catalysts: The Frontier between Homogeneous and Heterogeneous Catalysis. *Angew. Chem. Int. Ed.* **2005**, *44*, 7852–7872.
- (9) Lu, A.-H.; Salabas, E. L.; Schüth, F. Magnetic Nanoparticles: Synthesis, Protection, Functionalization, and Application. *Angew. Chem. Int. Ed.* **2007**, *46*, 1222–1244.
- (10) Gedanken, A. Using Sonochemistry for the Fabrication of Nanomaterials. *Ultrason. Sonochem.* **2004**, *11*, 47–55.
- (11) Rao, C. N. R.; Vivekchand, S. R. C.; Biswas, K.; Govindaraj, A. Synthesis of Inorganic Nanomaterials. *Dalton Trans.* **2007**, 3728–3749
- (12) Park, J.; Joo, J.; Kwon, S. G.; Jang, Y.; Hyeon, T. Synthesis of Monodisperse Spherical Nanocrystals. *Angew. Chem. Int. Ed.* **2007**, *46*, 4630–4660.
- (13) Pan, C.; Pelzer, K.; Philippot, K.; Chaudret, B.; Dassenoy, F.; Lecante, P.; Casanove, M.-J. Ligand-Stabilized Ruthenium Nanoparticles: Synthesis, Organization, and Dynamics. *J. Am. Chem. Soc.* **2001**, *123*, 7584–7593.
- (14) Aiken, J. D.; Finke, R. G. Polyoxoanion- and Tetrabutylammonium-Stabilized $Rh(0)_n$ Nanoclusters: Unprecedented Nanocluster Catalytic Lifetime in Solution. *J. Am. Chem. Soc.* **1999**, 121, 8803–8810
- (15) Quintanilla, A.; Butselaar-Orthlieb, V. C. L.; Kwakernaak, C.; Sloof, W. G.; Kreutzer, M. T.; Kapteijn, F. Weakly Bound Capping Agents on Gold Nanoparticles in Catalysis: Surface Poison? *J. Catal.* **2010**, *271*, 104–114.
- (16) Menard, L.; Xu, F.; Nuzzo, R.; Yang, J. Preparation of TiO₂-Supported Au Nanoparticle Catalysts from a Au₁₃ Cluster Precursor: Ligand Removal Using Ozone Exposure versus a Rapid Thermal Treatment. *J. Catal.* **2006**, *243*, 64–73.
- (17) Martra, G.; Prati, L.; Manfredotti, C.; Biella, S.; Rossi, M.; Coluccia, S. Nanometer-Sized Gold Particles Supported on SiO₂ by Deposition of Gold Sols from Au(PPh₃)₃Cl. *J. Phys. Chem. B* **2003**, 107, 5453–5459.
- (18) Mayer, A. B. R.; Mark, J. E. Transition Metal Nanoparticles Protected by Amphiphilic Block Copolymers as Tailored Catalyst Systems. *Colloid Polym. Sci.* **1997**, *275*, 333–340.
- (19) Lang, H.; May, R. A.; Iversen, B. L.; Chandler, B. D. Dendrimer-Encapsulated Nanoparticle Precursors to Supported Platinum Catalysts. *J. Am. Chem. Soc.* **2003**, *125*, 14832–14836.
- (20) Somorjai, G. A.; Frei, H.; Park, J. Y. Advancing the Frontiers in Nanocatalysis, Biointerfaces, and Renewable Energy Conversion by Innovations of Surface Techniques. *J. Am. Chem. Soc.* **2009**, *131*, 16589–16605.
- (21) Xian, J.; Hua, Q.; Jiang, Z.; Ma, Y.; Huang, W. Size-Dependent Interaction of the Poly(N -Vinyl-2-Pyrrolidone) Capping Ligand with Pd Nanocrystals. *Langmuir* **2012**, *28*, 6736–6741.
- (22) Antonietti, M.; Kuang, D.; Smarsly, B.; Zhou, Y. Ionic Liquids for the Convenient Synthesis of Functional Nanoparticles and Other Inorganic Nanostructures. *Angew. Chem. Int. Ed.* **2004**, 43, 4988–4992.

- (23) Dupont, J.; Scholten, J. D. On the Structural and Surface Properties of Transition-Metal Nanoparticles in Ionic Liquids. *Chem. Soc. Rev.* **2010**, 39, 1780–1804.
- (24) Neouze, M.-A. About the Interactions between Nanoparticles and Imidazolium Moieties: Emergence of Original Hybrid Materials. *J. Mater. Chem.* **2010**, 20, 9593–9607.
- (25) Verma, C.; Ebenso, E. E.; Quraishi, M. A. Transition Metal Nanoparticles in Ionic Liquids: Synthesisand Stabilization. *J. Mol. Liq.* **2019**, 276, 826–849.
- (26) He, Z.; Alexandridis, P. Nanoparticles in Ionic Liquids: Interactions and Organization. *Phys. Chem. Chem. Phys.* **2015**, *17*, 18238–18261.
- (27) Janiak, C. Ionic Liquids for the Synthesis and Stabilization of Metal Nanoparticles. Z. Naturforsch. 2013, 68, 1059–1089.
- (28) Baker, G. A.; Baker, S. N.; Pandey, S.; Bright, F. V. An Analytical View of Ionic Liquids. *Analyst* **2005**, *130*, 800–808.
- (29) Angell, C. A.; Byrne, N.; Belieres, J.-P. Parallel Developments in Aprotic and Protic Ionic Liquids: Physical Chemistry and Applications. *Acc. Chem. Res.* **2007**, *40*, 1228–1236.
- (30) Greaves, T. L.; Drummond, C. J. Protic Ionic Liquids: Properties and Applications. *Chem. Rev.* **2008**, *108*, 206–237.
- (31) Marsh, K. N.; Boxall, J. A.; Lichtenthaler, R. Room Temperature Ionic Liquids and Their Mixtures—a Review. *Fluid Phase Equilib.* **2004**, 219, 93–98.
- (32) Lodge, T. P. A Unique Platform for Materials Design. Science 2008, 321, 50-51.
- (33) Lin, Y.; Dehnen, S. [BMIm]₄[Sn₉Se₂₀]: Ionothermal Synthesis of a Selenidostannate with a 3D Open-Framework Structure. *Inorg. Chem.* **2011**, *50*, 7913–7915.
- (34) Pringle, J. M.; Golding, J.; Baranyai, K.; Forsyth, C. M.; Deacon, G. B.; Scott, J. L.; MacFarlane, D. R. The Effect of Anion Fluorination in Ionic Liquids—Physical Properties of a Range of Bis(Methanesulfonyl)Amide Salts. *New J. Chem.* **2003**, *27*, 1504—1510.
- (35) Ueki, T.; Watanabe, M. Macromolecules in Ionic Liquids: Progress, Challenges, and Opportunities. *Macromolecules* **2008**, *41*, 3739–3749.
- (36) Hallett, J. P.; Welton, T. Room-Temperature Ionic Liquids: Solvents for Synthesis and Catalysis. 2. *Chem. Rev.* **2011**, *111*, 3508–3576.
- (37) Torimoto, T.; Tsuda, T.; Okazaki, K.-i.; Kuwabata, S. New Frontiers in Materials Science Opened by Ionic Liquids. *Adv. Mater.* **2010**, *22*, 1196–1221.
- (38) Taubert, A.; Li, Z. Inorganic Materials from Ionic Liquids. Dalton Trans. 2007, 723-727.
- (39) Firestone, M. A.; Dietz, M. L.; Seifert, S.; Trasobares, S.; Miller, D. J.; Zaluzec, N. J. Ionogel-Templated Synthesis and Organization of Anisotropic Gold Nanoparticles. *Small* **2005**, *1*, 754–760.
- (40) Fonseca, G. S.; Umpierre, A. P.; Fichtner, P. F. P.; Teixeira, S. R.; Dupont, J. The Use of Imidazolium Ionic Liquids for the Formation and Stabilization of Ir⁰ and Rh⁰ Nanoparticles: Efficient Catalysts for the Hydrogenation of Arenes. *Chem. Eur. J.* **2003**, *9*, 3263–3269
- (41) Migowski, P.; Zanchet, D.; Machado, G.; Gelesky, M. A.; Teixeira, S. R.; Dupont, J. Nanostructures in Ionic Liquids: Correlation of Iridium Nanoparticles' Size and Shape with Imidazolium Salts' Structural Organization and Catalytic Properties. *Phys. Chem. Chem. Phys.* **2010**, *12*, 6826–6833.
- (42) Anderson, K.; Cortiñas Fernández, S.; Hardacre, C.; Marr, P. C. Preparation of Nanoparticulate Metal Catalysts in Porous Supports Using an Ionic Liquid Route; Hydrogenation and C–C Coupling. *Inorg. Chem. Commun.* **2004**, *7*, 73–76.
- (43) Weingärtner, H. Understanding Ionic Liquids at the Molecular Level: Facts, Problems, and Controversies. *Angew. Chem. Int. Ed.* **2008**, 47, 654–670.
- (44) Dupont, J. On the Solid, Liquid and Solution Structural Organization of Imidazolium Ionic Liquids. *J. Braz. Chem. Soc.* **2004**, *15*, 341–350.

- (45) Kobrak, M. N.; Li, H. Electrostatic Interactions in Ionic Liquids: The Dangers of Dipole and Dielectric Descriptions. *Phys. Chem. Chem. Phys.* **2010**, *12*, 1922–1932.
- (46) Zhang, H.; Cui, H. Synthesis and Characterization of Functionalized Ionic Liquid-Stabilized Metal (Gold and Platinum) Nanoparticles and Metal Nanoparticle/Carbon Nanotube Hybrids. *Langmuir* **2009**, 25, 2604–2612.
- (47) Ostwald, W. Blocking of Ostwald Ripening Allowing Long-Tern Stabilization. *Phys. Chem.* **1901**, *37*, 385.
- (48) Marquardt, D.; Xie, Z.; Taubert, A.; Thomann, R.; Janiak, C. Microwave Synthesis and Inherent Stabilization of Metal Nanoparticles in 1-Methyl-3-(3-Carboxyethyl)-Imidazolium Tetrafluoroborate. *Dalton Trans.* **2011**, *40*, 8290–8293.
- (49) Redel, E.; Thomann, R.; Janiak, C. First Correlation of Nanoparticle Size-Dependent Formation with the Ionic Liquid Anion Molecular Volume. *Inorg. Chem.* **2008**, *47*, 14–16.
- (50) Ott, L. S.; Finke, R. G. Nanocluster Formation and Stabilization Fundamental Studies:† Investigating "Solvent-Only" Stabilization En Route to Discovering Stabilization by the Traditionally Weakly Coordinating Anion BF₄⁻ Plus High Dielectric Constant Solvents. *Inorg. Chem.* **2006**, *45*, 8382–8393.
- (51) Li, Z.; Friedrich, A.; Taubert, A. Gold Microcrystal Synthesis via Reduction of HAuCl₄ by Cellulose in the Ionic Liquid 1-Butyl-3-Methyl Imidazolium Chloride. *J. Mater. Chem.* **2008**, *18*, 1008–1014.
- (52) Vollmer, C.; Redel, E.; Abu-Shandi, K.; Thomann, R.; Manyar, H.; Hardacre, C.; Janiak, C. Microwave Irradiation for the Facile Synthesis of Transition-Metal Nanoparticles (NPs) in Ionic Liquids (ILs) from Metal—Carbonyl Precursors and Ru-, Rh-, and Ir-NP/IL Dispersions as Biphasic Liquid—Liquid Hydrogenation Nanocatalysts for Cyclohexene. *Chem.—Eur. J.* **2010**, *16*, 3849—3858.
- (53) Zhu, J.; Shen, Y.; Xie, A.; Qiu, L.; Zhang, Q.; Zhang, S. Photoinduced Synthesis of Anisotropic Gold Nanoparticles in Room-Temperature Ionic Liquid. *J. Phys. Chem. C* **2007**, *111*, 7629–7633.
- (54) Kim, K.; Lang, C.; Kohl, P. The Role of Additives in the Electroreduction of Sodium Ions in Chloroaluminate-Based Ionic Liquids. J. Electrochem. Soc. 2005, 152, E9–E13.
- (55) Safavi, A.; Maleki, N.; Tajabadi, F.; Farjami, E. High Electrocatalytic Effect of Palladium Nanoparticle Arrays Electrodeposited on Carbon Ionic Liquid Electrode. *Electrochem. Commun.* **2007**, *9*, 1963–1968.
- (56) Peppler, K.; Pölleth, M.; Meiss, S.; Rohnke, M.; Janek, J. Electrodeposition of Metals for Micro- and Nanostructuring at Interfaces between Solid, Liquid and Gaseous Conductors: Dendrites, Whiskers and Nanoparticles. Z. Phys. Chem. 2006, 220, 1507–1527.
- (57) Rohan, A. L.; Switzer, J. R.; Flack, K. M.; Hart, R. J.; Sivaswamy, S.; Biddinger, E. J.; Talreja, M.; Verma, M.; Faltermeier, S.; Nielsen, P. T.; et al. The Synthesis and the Chemical and Physical Properties of Non-Aqueous Silylamine Solvents for Carbon Dioxide Capture. *ChemSusChem* **2012**, *5*, 2181–2187.
- (\$8) Ethier, A. L.; Hart, E. C.; Saunders, S. R.; Biddinger, E. J.; Fadhel, A. Z.; Dilek, C.; Pollet, P.; Eckert, C. A.; Liotta, C. L. Reversible Ionic Surfactants for Gold Nanoparticle Synthesis. *Green Mater.* **2014**, *2*, 54–61.
- (59) Eckert, C.; Liotta, C. Reversible Ionic Liquids as Double-Action Solvents for Efficient CO2 Capture: Atlanta, 2011.
- (60) Pollet, P.; Eckert, C. A.; Liotta, C. L. Solvents for Sustainable Chemical Processes. WIT Trans. Ecol. Environ. 2011, 154, 21–31.
- (61) Bryant, K.; Ibrahim, G.; Saunders, S. R. Switchable Surfactants for the Preparation of Monodisperse, Supported Nanoparticle Catalysts. *Langmuir* **2017**, 33, 12982–12988.
- (62) Bryant, K.; West, C. W.; Saunders, S. R. Impacts of Calcination on Surface-Clean Suppported Nanoparticles. *Appl. Catal., A* **2019**, 579, 58–64.
- (63) Liu, J.; Cheng, S.; Zhang, J.; Feng, X.; Fu, X.; Han, B. Reverse Micelles in Carbon Dioxide with Ionic-Liquid Domains. *Angew. Chem. Int. Ed.* **2007**, *46*, 3313–3315.
- (64) Spirin, M. G.; Brichkin, S. B.; Razumov, V. F. Growth Kinetics for AgI Nanoparticles in AOT Reverse Micelles: Effect of Molecular

- Length of Hydrocarbon Solvents. J. Colloid Interface Sci. 2008, 326, 117-120.
- (65) Richard, B.; Lemyre, J.-L.; Ritcey, A. M. Nanoparticle Size Control in Microemulsion Synthesis. *Langmuir* **2017**, 33, 4748–4757.
- (66) Sharma, S.; Yadav, N.; Chowdhury, P. K.; Ganguli, A. K. Controlling the Microstructure of Reverse Micelles and Their Templating Effect on Shaping Nanostructures. *J. Phys. Chem. B* **2015**, *119*, 11295–11306.
- (67) López-Quintela, M. A.; Tojo, C.; Blanco, M. C.; García Rio, L.; Leis, J. R. Microemulsion Dynamics and Reactions in Microemulsions. *Curr. Opin. Colloid Interface Sci.* **2004**, *9*, 264–278.
- (68) Granata, G.; Pagnanelli, F.; Nishio-Hamane, D.; Sasaki, T. Effect of Surfactant/Water Ratio and Reagents' Concentration on Size Distribution of Manganese Carbonate Nanoparticles Synthesized by Microemulsion Mediated Route. *Appl. Surf. Sci.* 2015, 331, 463–471.
- (69) Khan, M. F.; Singh, M. K.; Sen, S. Measuring Size, Size Distribution, and Polydispersity of Water-in-Oil Microemulsion Droplets Using Fluorescence Correlation Spectroscopy: Comparison to Dynamic Light Scattering. *J. Phys. Chem. B* **2016**, *120*, 1008–1020.
- (70) Graham, T. R.; Renslow, R.; Govind, N.; Saunders, S. R. Precursor Ion-Ion Aggregation in the Brust-Schiffrin Synthesis of Alkanethiol Nanoparticles. J. Phys. Chem. C 2016, 120, 19837—19847.
- (71) Stejskal, E. O.; Tanner, J. E. Spin Diffusion Measurements: Spin Echoes in the Presence of a Time-Dependent Field Gradient. *J. Chem. Phys.* **1965**, 42, 288–292.
- (72) Macchioni, A.; Ciancaleoni, G.; Zuccaccia, C.; Zuccaccia, D. Determining Accurate Molecular Sizes in Solution through NMR Diffusion Spectroscopy. *Chem. Soc. Rev.* **2008**, *37*, 479–489.
- (73) Chen, S. H.; Wei, S. K.-H. Modification of the Stokes–Einstein Equation with a Semiempirical Microfriction Factor for Correlation of Tracer Diffusivities in Organic Solvents. *Ind. Eng. Chem. Res.* **2011**, *50*, 12304–12310.
- (74) Eastoe, J.; Hollamby, M. J.; Hudson, L. Recent Advances in Nanoparticle Synthesis with Reversed Micelles. *Adv. Colloid Interface Sci.* **2006**, 128–130, 5–15.
- (75) López-Quintela, M. A.; Tojo, C.; Blanco, M. C.; García Rio, L.; Leis, J. R. Microemulsion Dynamics and Reactions in Microemulsions. *Curr. Opin. Colloid Interface Sci.* **2004**, *9*, 264–278.
- (76) Tukey, J. W. Exploratory Data Analysis; Mosteller, F., Ed.; Addison-Wesley Publishing Company, 1977; pp 5–24.
- (77) Fumino, K.; Fossog, V.; Wittler, K.; Hempelmann, R.; Ludwig, R. Dissecting Anion—Cation Interaction Energies in Protic Ionic Liquids. *Angew. Chem. Int. Ed.* **2013**, *52*, 2368–2372.